

Track-weighted imaging methods: extracting information from a streamlines tractogram

Fernando Calamante^{1,2,3} 

Received: 11 October 2016 / Revised: 22 January 2017 / Accepted: 23 January 2017 / Published online: 8 February 2017
© ESMRMB 2017

Abstract A whole-brain streamlines data-set (so-called tractogram) generated from diffusion MRI provides a wealth of information regarding structural connectivity in the brain. Besides visualisation strategies, a number of post-processing approaches have been proposed to extract more detailed information from the tractogram. One such approach is based on exploiting the information contained in the tractogram to generate track-weighted (TW) images. In the track-weighted imaging (TWI) approach, a very large number of streamlines are often generated throughout the brain, and an image is then computed based on properties of the streamlines themselves (e.g. based on the number of streamlines in each voxel, or their average length), or based on the values of an associated image (e.g. a diffusion anisotropy map, a T_2 map) measured at the coordinates of the streamlines. This review article describes various approaches used to generate TW images and discusses the flexible formalism that TWI provides to generate a range of images with very different contrast, as well as the super-resolution properties of the resulting images. It also explains how this approach provides a powerful means to study structural and functional connectivity simultaneously. Finally, a number of key issues for its practical implementation are discussed.

Keywords Fibre-tracking · Tractogram · Super-resolution · Connectivity · Tractography

Introduction

Diffusion MRI data can provide an estimate of the local white matter fibre orientations non-invasively, which in turn can be used with a fibre-tracking algorithm to reconstruct a representation of the white matter pathways in the brain [1]. Currently, the most commonly used fibre-tracking algorithms are based on generating a set of streamlines,¹ an algorithm also known as deterministic streamlines [2, 3] or probabilistic streamlines [4], depending on how the streamlines propagation is carried out [1].

In the particular case of whole-brain tracking, streamlines are most often seeded throughout the white matter, thus providing an overall representation of white matter pathways throughout the brain (the so-called “tractogram”—see Fig. 1). Note that, in practice, a whole-brain tractogram can also be generated with other seeding strategies, such as seeding throughout the grey matter/white matter interface.

Besides a number of visualisation strategies to display and interrogate the resulting tractogram (i.e. the set of streamlines), various post-processing approaches have been proposed to extract more detailed information (and, often, quantitative information) from the set of streamlines. For

✉ Fernando Calamante
fernando.calamante@floreys.edu.au

¹ Florey Institute of Neuroscience and Mental Health, Melbourne Brain Centre, 245 Burgundy Street, Heidelberg, VIC 3084, Australia

² Florey Department of Neuroscience and Mental Health, University of Melbourne, Melbourne, VIC, Australia

³ Department of Medicine, Austin Health and Northern Health, University of Melbourne, Melbourne, VIC, Australia

¹ Throughout this work, the terms “streamline” and “track” are used interchangeably, to represent a mathematical representation (i.e. a three-dimensional curve generated using a tractography algorithm). In contrast, the terms “tract” and “white matter pathway” are also used interchangeably to represent the actual biological structure in the brain.

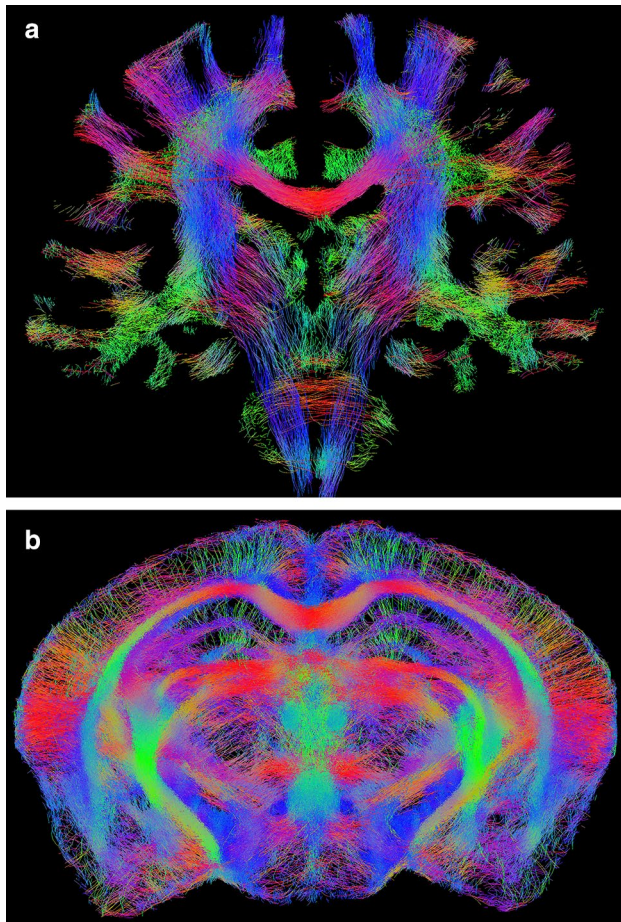


Fig. 1 Example whole-brain tractograms (100,000 probabilistic streamlines). **a** 4-mm coronal section of the tractogram from a human healthy subject scanned at 3 T. **b** 0.2-mm coronal section of the tractogram from an ex vivo mouse brain scanned at 16.4 T. The *colour-coding* indicates the local fibre orientation (*red* left–right, *green* dorsal–ventral, *blue* cranial–caudal). **b** Is modified from a figure previously published in [24], with permission of Elsevier Inc., 2012

example, the tractogram has been used to estimate the degree of structural connectivity between brain regions [5, 6], i.e. an estimate of the density of white matter connections between regions of the brain grey matter; this type of application includes what it has now become the very active research field of connectomics [7, 8], or the study of the brain connectome. The connectivity information has also been exploited to guide tissue parcellation, such as in the seminal work by Behrens and colleagues to parcellate the human thalamus based on its connectivity to cortical regions [5].

The streamlines corresponding to a given white matter pathway also can be isolated to define a “tract of interest” (TOI)² [9, 10], which can be subsequently used to measure

² The TOI is equivalent to the commonly used region of interest (ROI), for the particular case that its extent is determined by the volume occupied by a set of streamlines (typically corresponding to a given white matter structure).

tract-specific average diffusion MRI properties, such as the mean tract value of the average diffusivity, the diffusion anisotropy, or even of other non-diffusion MRI parameter (such as the mean tract value for T_2). While this approach can be used to obtain a tract-specific quantitative value, it cannot characterise the possible heterogeneity that can be present within the white matter pathway. To address this important limitation, a bootstrap method was applied to determine the distribution of diffusion metrics (e.g. the fractional anisotropy, FA), and encode this information at each point along the streamline, with the pointwise assessment of streamline tractography attributes (PASTA) method [11]. Related approaches to extend these ideas have been also proposed to generate tract “profiles” of MRI parameters (i.e. their values at multiple locations along their trajectories) for all the streamlines in a given white matter structure [12–14], which can be subsequently used, for example, for quantitative comparison of a patient group vs. a control group [15].

A completely different strategy to extract other information from streamlines relied on quantifying the shape of the streamlines (e.g. their curvature, torsion), as well as a measure of the relative spatial configuration between pairs of curves [16], i.e. a number of features related to geometrical properties of the streamlines.

The information contained in a whole-brain tractogram can also be exploited to generate track-weighted (TW) images [17]. In this track-weighted imaging (TWI) approach, a TW image can be generated either based on properties of the streamlines themselves (e.g. based on the number of streamlines in each voxel [18–21], their average length [22]), or based on the values of an associated image/map (e.g. a diffusion anisotropy map) measured at the coordinates of the streamlines [17]. This review article describes various approaches used to generate TW images, and discuss the flexible formalism that TWI provides to generate a range of images with very different contrast, as well as the super-resolution properties of the resulting images. This review article also explains how this approach provides a very powerful means to study structural and functional connectivity simultaneously. Finally, a number of key issues for its practical implementation are discussed.

TW images based solely on properties of the tractogram

Possibly one of the simplest TWI variants correspond to computing the number of streamlines traversing each voxel and assigning that value as the intensity of the TW image [18–21]; this approach is equivalent to a “histogram map” of the streamline count, where voxels are equivalent to the histogram bins. This type of TW image is known as anatomical connectivity mapping (ACM) [18, 20],

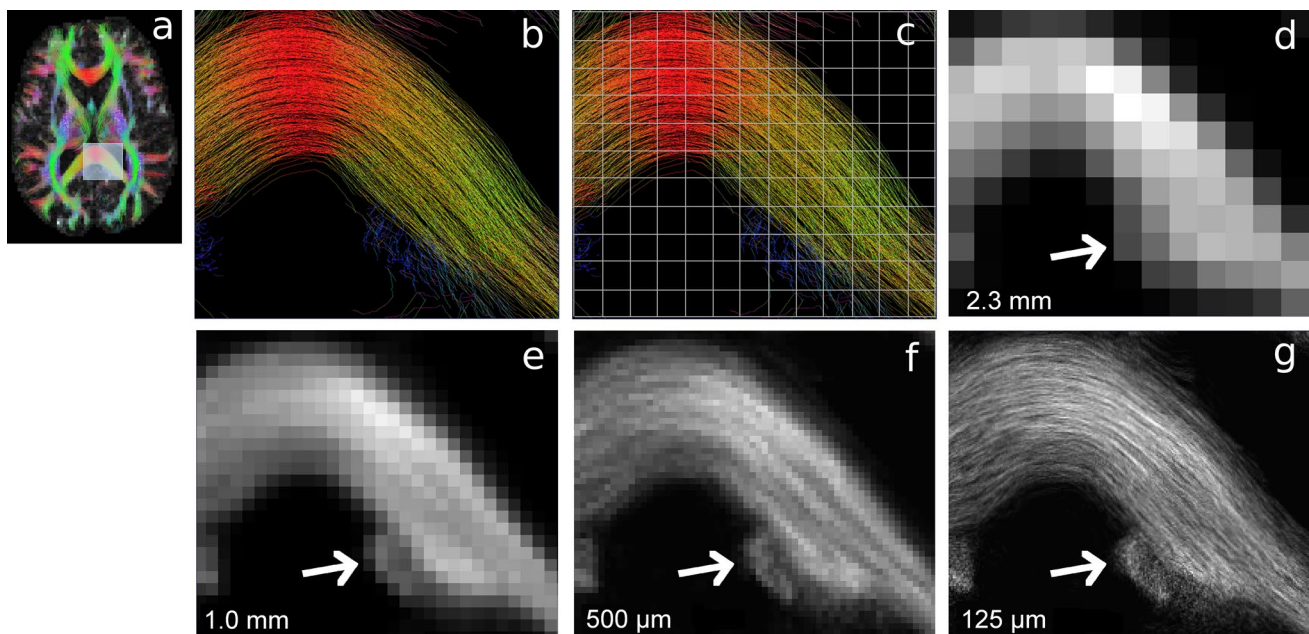


Fig. 2 Illustration of the track-density imaging (TDI) formation and the super-resolution principle. **a** Axial slice of the tractogram highlighting the region that is shown as zoomed version in **b–g**. **b** Zoomed tractogram; **c** zoomed tractogram with a grid-size of native acquired resolution (2.3 mm isotropic for the diffusion MRI data used here); **d** TDI map without super-resolution (i.e. at native resolution) calculated by counting the number of streamlines within each grid element. The same procedure as in **b–d** can be repeated with grid-

sizes of smaller resolution to achieve super-resolution. The *bottom row* shows the corresponding super-resolution TDI maps calculated at 1 mm (**e**), 500 μm (**f**), and 125 μm (**g**) isotropic resolutions. All TDI maps were calculated based on the same tractogram, they just differ in the choice of grid-size. As can be appreciated in the figure, brain structures (e.g. the cingulum bundle, see *arrow*) are visualised with increasing detail by using finer super-resolution

track-density image (TDI) [19], or fibre density mapping (FDM) [21]. While ACM and FDM were introduced as quantitative measures of anatomical connectivity and the density of white matter fibres, respectively, TDI was introduced as a qualitative imaging method with high anatomical contrast. Importantly, TDI not only has been found to have high anatomical contrast, but it has been also shown to have super-resolution properties [23], such that its spatial resolution can be higher than that of the acquired diffusion MRI data (see Fig. 2).³ The continuity of the tracks provides extra information from outside the voxel to disentangle the intra-voxel localisation of the streamlines and thus generate sub-voxel information (see Fig. 3).⁴ For example, high contrast super-resolution TDI maps of the in vivo human brain at 0.125 mm isotropic resolution were constructed from diffusion MRI data acquired at 2.3 mm isotropic resolution [19] (see also Fig. 4a), and 0.02 mm isotropic TDI maps of the ex vivo mouse brain were constructed from diffusion MRI data acquired at 0.1 mm resolution (see Fig. 4b) [24]. The

super-resolution properties of TDI were validated by using in silico phantoms, as well as by comparing the super-resolution TDI maps generated from down-sampled high-resolution 7 T diffusion MRI data to TDI maps generated at native resolution (i.e. without super-resolution) from the original high-resolution acquired data [23]. It is also important to emphasise that this super-resolution property is not equivalent to image interpolation, as demonstrated in [19] (e.g. see Fig. 8 in that article).

It should be noted that, in practice, there are several ways to consider the contribution from streamlines to the total count in TDI. For example, the streamlines traversing a voxel can be counted in a binary way, all contributing a unit value regardless of their length within the voxel. Alternatively, the contribution of each streamline can be weighted by the length of the streamline segment within the voxel. The TDI results shown here correspond to the former case.

An interesting feature of the TDI maps is that their signal-to-noise ratio was shown to be influenced, not only by the acquisition parameters (as expected), but also by the total number of streamlines generated in the tractogram and by the size of the super-resolution voxel [19]. This provides a means to increase the quality of the final TDI map (for a given diffusion MRI data set) simply by post-processing

³ ACM and FDM are essentially similar to TDI at native resolution (i.e. without applying super-resolution).

⁴ In the TDI analogy as a histogram map, super-resolution can be seen as the fact that the bin size (i.e. voxel size) can be, to some extent, arbitrarily chosen.

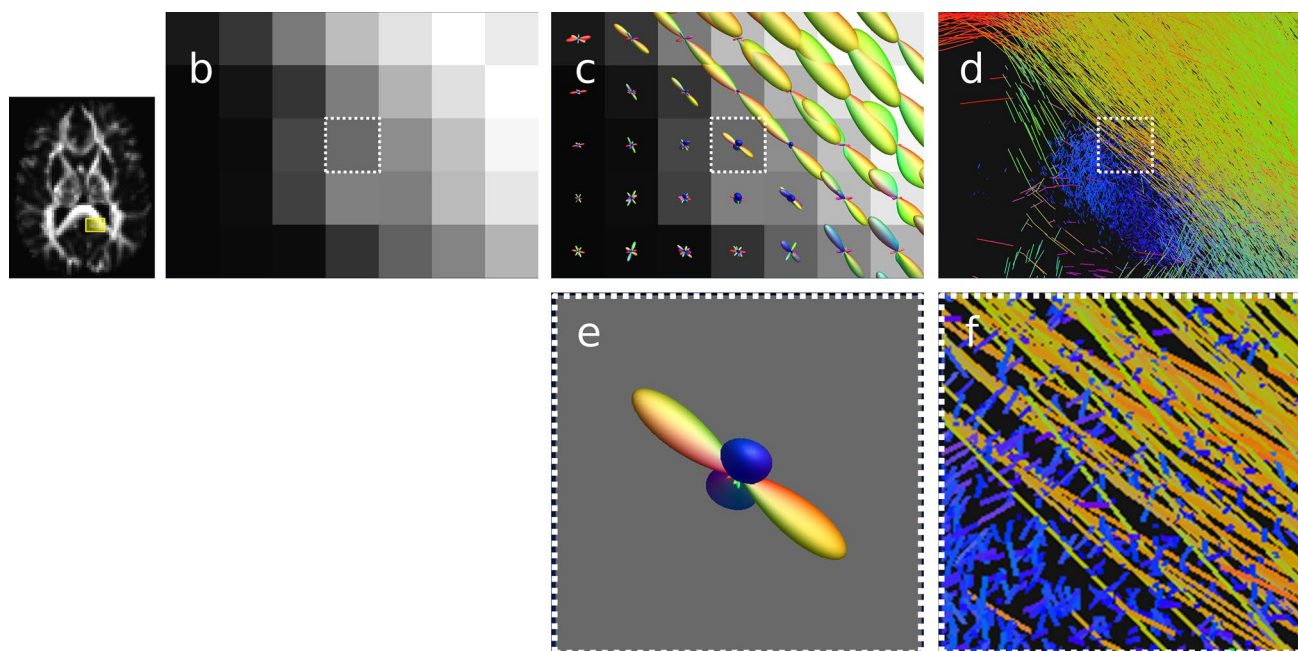


Fig. 3 Illustration of the origin of the super-resolution property. **a** Axial slice of a TDI map calculated at native resolution (2.3 mm isotropic for the diffusion MRI data used here), highlighting the region that is shown as zoomed version in **b–d**. **b** Zoomed TDI map at native resolution; the highlighted voxel is shown as zoomed version in **e–f**. **c** Same image as in **b**, but with the fibre orientation distribution (FOD) overlain in each voxel. **d** Corresponding region of the tractogram. **e** Zoomed version of the voxel highlighted in (c); the FOD data identified two fibre populations within the voxel: one corresponding to the

corpus callosum (in yellow) and the other to the cingulum bundle (in blue). Based on these FOD data, it is not possible to determine where within the voxel these fibre populations are located. **f** Zoomed version of the voxel highlighted in **d**; the continuity of the streamlines provide sub-voxel information, and it is now possible to disentangle the spatial distribution of the corpus callosum and cingulum bundle within the voxel. This is the source of the super-resolution property in TDI, i.e. the streamlines provide sub-voxel localisation

and, therefore, a means to change the contrast-to-noise ratio without involving an increased acquisition time (see Fig. 5 for an example). The signal-to-noise ratio for a given total number of tracks depends on a number of factors, including the signal-to-noise ratio of the diffusion MRI data, the number of diffusion gradient directions, b value, and super-resolution voxel size [19]; the rate of increase is expected to be relatively much slower when using very large number of streamlines (e.g. see the shape of the curve in Fig. 5). As can be seen in the example TDI maps in Fig. 5, for low number of tracks the image is very “patchy” (because not enough tracks have been generated to sufficiently populate the super-resolution voxels), leading to very low signal-to-noise ratio. This is equivalent to a histogram having a noisy appearance when using a low number of data samples. As it is also the case for the histogram, when a very large number of samples have been considered (large relative to the histogram bin, or for our case, to the super-resolution voxel-size), then the change of the histogram appearance with further increases in the number of data samples is not so apparent.

Furthermore, analogous to the directionally encoded colour (DEC) maps in diffusion tensor imaging [25], fibre directionality information can be incorporated into the

super-resolution TDI maps, by assigning an RGB colour to each spatial direction; for example, the colour in each voxel can be determined by averaging the colours of all the streamline segments contained within the voxel (see Fig. 6) [19]. Importantly, it was shown that DEC-TDI maps not only have super-resolution properties, but also provide an improved representation of the colour-encoding in areas of multiple fibre populations compared with DEC maps from diffusion tensor imaging, given that they have a better behaved definition of the colour choice [17]. In areas of crossing fibres, the DEC-FA map (with its colour determined by the orientation of the eigenvector corresponding to the major eigenvalue) can show low colour coherence (due to the noise sensitivity of the eigenvector direction), while this is avoided in DEC-TDI, i.e. averaging colours of the streamlines in a voxel is better behaved with respect to noise than choosing the colour of the computed major eigenvector (e.g. see Fig. 7 in Ref. [17]). More recently, an approach that also avoids these uncertainties with colour-encoding in crossing fibre areas has been proposed, based on the information contained in the fibre orientation distribution (FOD) [26]; this approach does not require reconstruction of a tractogram; therefore, it cannot use the super-resolution properties of DEC-TWI.

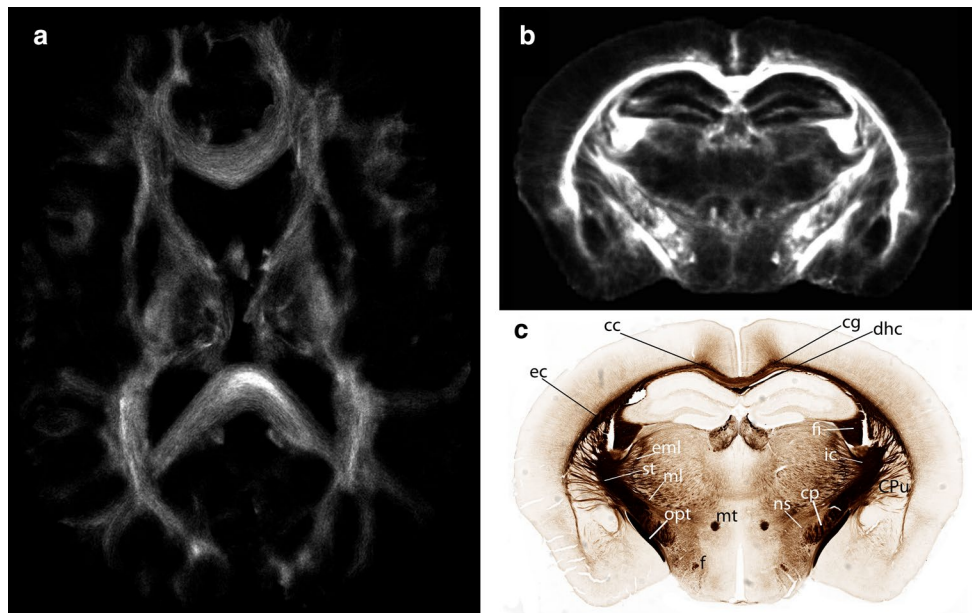


Fig. 4 Example super-resolution TDI maps. **a** TDI map of the in vivo human brain at 0.125 mm isotropic resolution (constructed from diffusion MRI data acquired at 2.3 mm resolution on a 3 T scanner). **b** TDI map of the ex vivo mouse brain at 0.02 mm isotropic resolution (constructed from diffusion MRI data acquired at 0.1 mm resolution on a 16.4 T scanner). **c** Myelin staining of the same mouse brain, with a number of structures labelled. *cc* corpus callosum, *cg* cingulum, *cp*

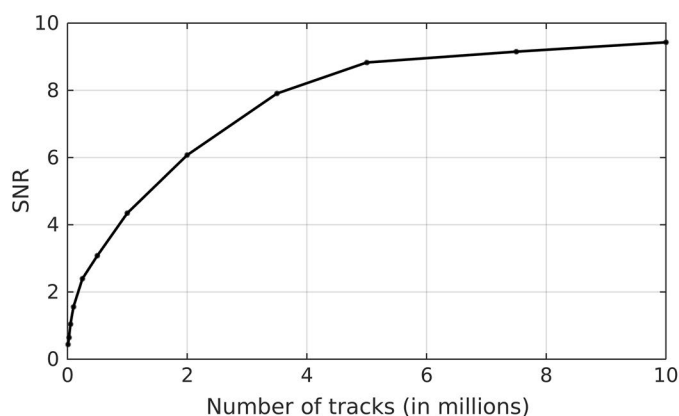
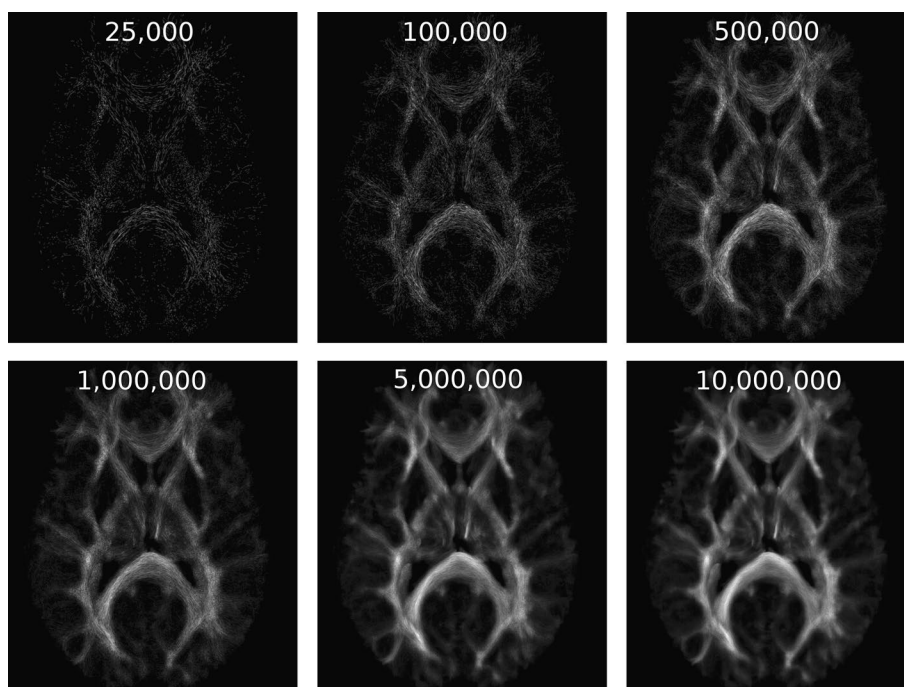
cerebral peduncle, *CPu* caudate putamen (striatum), *dhc* dorsal hippocampal commissure, *ec* external capsule, *eml* external medullary lamina, *f* fornix, *fi* fimbria of the hippocampus, *ic* internal capsule, *ml* medial lemniscus, *mt* mammillothalamic tract, *ns* nigrostriatal tract, *opt* optic tract, *st* stria terminalis. **b**, **c** Modified from a figure previously published in [24], with permission of Elsevier Inc., 2012

In order to investigate whether the very high anatomical contrast provided by super-resolution TDI maps is meaningful, the anatomical information from these maps was compared with that from high-resolution T_1 -weighted images from in vivo 7T human MRI data [27], and with histology for ex vivo ultra-high field mouse brain MRI (e.g. see Fig. 4) [24]. These studies demonstrated the very useful anatomical information contained in TDI maps. In particular, the high anatomical contrast in TDI and DEC-TDI maps has been exploited, for example, to develop a detailed white matter atlas of the in vivo human brain [28], to characterise the structures within the brain stem [29, 30], and to precisely define seed regions for tractography [19, 31], as well as to visualise the mouse barrel cortex [32], map the somatosensory connectivity in the ex vivo mouse brain [33], and provide an enhanced characterisation of zebrafish [34] and zebra finch [35] brains.

Given that TDI is essentially a map of the tractogram, the better the quality of the fibre-tracking results, the better quality of the resulting TDI map. For example, increasing the amount of data (e.g. increasing the number of diffusion-weighted encoding directions), or increasing the signal-to-noise ratio of the data (e.g. by using better RF coils, stronger gradients) can all lead to better fibre-tracking results. Similarly, the use of advanced models to estimate fibre orientations within

a voxel [36, 37] can lead to more meaningful anatomical information (see Fig. 7), and the use of better fibre-tracking algorithms [38–41] can lead to improved tractograms. As illustration, the high-quality diffusion MRI data from the Human Connectome Project [42, 43], when combined with advanced models to estimate fibre orientations [44] and state-of-the-art fibre-tracking strategies [38, 45] generates very high quality DEC-TDI maps, i.e. maps with very high anatomical detail, spatial resolution, and contrast-to-noise ratio (e.g. see Fig. 8). Similarly, very impressive super-resolution TDI maps can be achieved based on ex vivo brain imaging at ultra-high field MRI: the features that can be visualised using super-resolution TDI and DEC-TDI can be outstanding, because long acquisition times can be employed to acquire very high resolution and high signal-to-noise ratio diffusion MRI data. For example, TDI maps were used as a tool to visualise the barrel cortex in the ex vivo mouse brain, based on data acquired at 16.4T, and the identified barrel structure corresponded well with that seen in histology [32]. Similarly, ultra-high field MRI of the ex vivo zebrafish brain were used to generate 5 μm isotropic resolution DEC-TDI maps [34], which provided a rich visualisation of numerous anatomical structures, including 17 structures previously unidentifiable using MR microimaging.

Fig. 5 Illustration of the effect of number of streamlines in the signal-to-noise ratio (SNR) of the TDI map. The *top* two rows show six TDI maps (0.3 mm isotropic resolution) created with increasing number of streamlines (as indicated by the numbers in each figure). All TDI maps were generated using the same diffusion MRI data (2.5 mm isotropic, 60 diffusion-encoding directions, $b = 3000 \text{ s/mm}^2$, acquired on a 3T scanner), and they only differ in the total number of streamlines used to construct the tractogram. It can be clearly seen that increasing the number of streamlines increases the quality of the TDI maps (e.g. their SNR). To quantify this effect, a plot of SNR vs. number of tracks is shown in the *bottom*, which was calculated for a *rectangular* region of interest (368 voxels in size) manually drawn in the splenium of the corpus callosum in the slice shown in the figure. The plot confirms the SNR increase with increasing number of tracks, with SNR defined as the mean divided by the standard deviation of the TDI values within the region



Anatomical contrast vs. quantitation

The most commonly used method for seeding when generating a whole-brain tractogram is to distribute the seeds throughout the white matter; this leads to a length-bias in the streamline density: longer white matter pathways will have a larger number of seeds, which generate a larger number of streamlines, which in turn produce higher signal intensity in TDI maps. This source of bias is in fact an important source of anatomical contrast in TDI. While other sources of tracking bias provide no anatomical useful information (e.g. the bias towards tracking the medial aspect of the corpus callosum projections when using diffusion tensor imaging—see Fig. 7c), the length-bias in tracking can help differentiate neighbouring white matter structures based on their tract length—a useful characteristic when one is interested in anatomical contrast. On the other hand, there are some scenarios when one may want to

avoid the above mentioned length-bias. For example, when investigating short white matter structures [24, 29, 32, 33], it is beneficial to minimise the dominant high-contrast signal from long fibres. Similarly, for DEC-TDI maps, whose contrast is primarily given by the orientation information, it is also beneficial to reduce the length-bias effect in order to avoid colour saturation of long white matter structures [24]. A number of strategies have been proposed to minimise this length-bias effect, i.e. the over-representation of long white matter pathways. These include two variants to the original TDI method: (1) the technique known as length-scaled TDI (*lsTDI*), in which the contribution of each streamline to the final track-count value is scaled by the inverse of its length [23], and (2) short-tracks TDI (*stTDI*), in which a standard TDI map is computed, but based on a tractogram that was generated by constraining the tracking to propagate streamlines up to a given maximum length (e.g. 10 times the acquired voxel size) [24]. An alternative approach to

Fig. 6 **a** Fractional anisotropy (FA) map from a healthy volunteer (2.3 mm isotropic diffusion MRI acquired at 3T). **b** Directional-encoded colour (DEC) FA map. **c** Super-resolution track-density imaging (TDI) map at 0.25 mm isotropic resolution, created using one million streamlines. **d** Super-resolution DEC-TDI map (0.25 mm resolution). Note that all maps were created based on the same acquired diffusion MRI data, but they differ in the way the data were post-processed. The *color-coding* corresponds to the main local orientation (*red* left–right, *green* anterior–posterior, *blue* inferior–superior), as defined by the orientation of the major eigenvector of the diffusion tensor (for **b**) or the orientation of the streamlines within the voxel (for **d**)

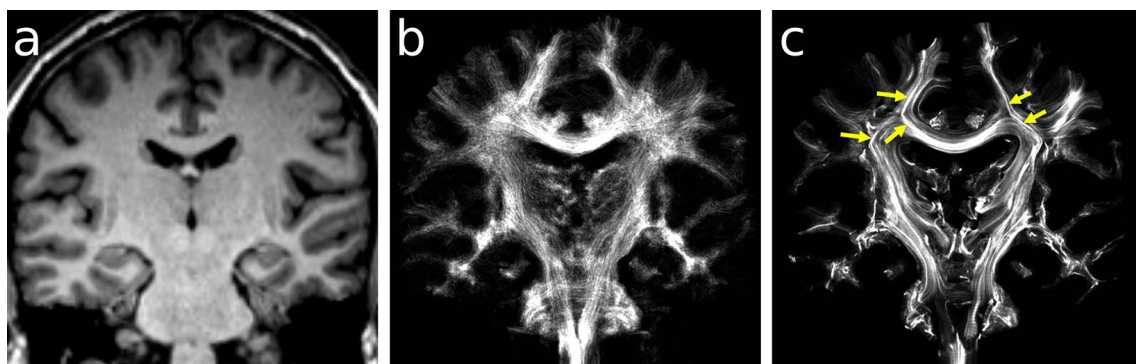
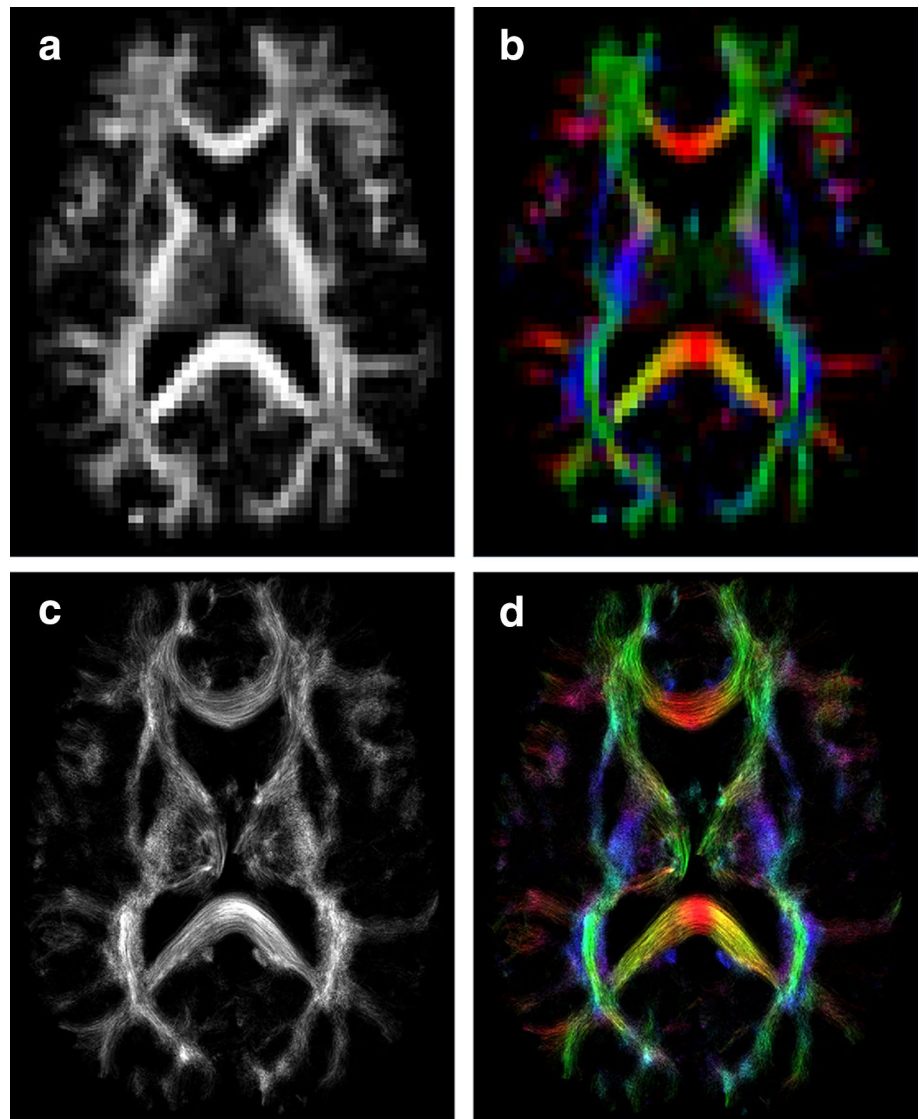
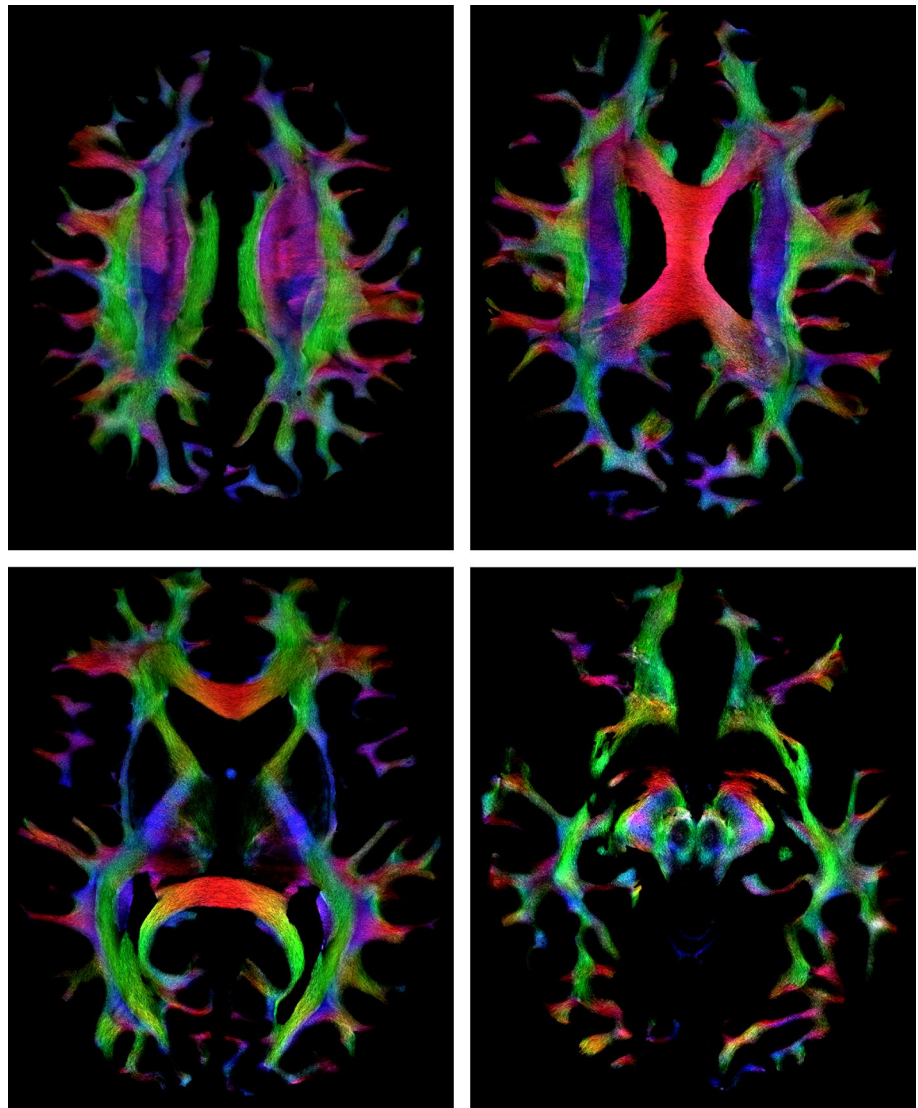


Fig. 7 Illustration of the effect of the tractography method on TDI contrast. **a** Coronal T₁-weighted image for anatomical localisation. **b** Super-resolution track-density imaging (TDI) map generated using constrained spherical deconvolution (to model the intra-voxel fibre orientations) and probabilistic streamlines. **c** Corresponding super-

resolution TDI map generated using the tensor model and deterministic streamlines. All TDI maps were generated using one million tracks and 0.25 mm isotropic resolution (based on the same 2.3 mm acquired diffusion MRI data). The *arrows* in **c** indicate areas artificially enhanced due to tractography-related errors and biases

Fig. 8 Example high-quality super-resolution directional-encoded colour (DEC) track-density imaging (TDI) maps calculated based on 1.25 mm resolution diffusion MRI data, acquired as part of the Human Connectome Project [42, 43]. The tractogram (10 million streamlines) used to compute the DEC-TDI maps was calculated using advanced models to estimate the fibre orientations within a voxel [44], and state-of-the-art fibre-tracking algorithms that incorporate anatomical information [38] and are quantitative [45]. *Red* left–right, *green* anterior–posterior, *blue* inferior–superior. Figure constructed from fibre-tracking data kindly provided by Dr. Chun-Hung Yeh (The Florey Institute of Neuroscience and Mental Health, Melbourne, Australia)



minimise the length-bias effect is to use one of the tracking methods that have been specifically designed to make tractograms more quantitative [38–41, 46–48]. It should be noted, however, that length-bias is not the only possible source of bias in fibre-tracking. Other sources of bias and/or errors include curvature, dispersion, the so-called fibre crossing vs. kissing effect, seeding strategy, and termination criteria [1, 38, 39, 41, 48–50]. The reader is referred to these references for further details on tractography biases and methods to reduce them.

While super-resolution TDI was initially developed primarily as a qualitative imaging method with high anatomic contrast [19], track-count mapping techniques have been appealing as a tool that provides a potential surrogate measure of white matter “fibre density” and, therefore, as a quantitative parameter. There has been, however, some controversy regarding the quantitative properties of track-count mapping. While a number of studies have reported

very interesting applications, such as to tumours [21, 51, 52], Parkinson’s disease [53], Alzheimer’s disease [20, 54], multiple sclerosis [55, 56], traumatic brain injury [57], stroke [58], brain development [59], pain syndromes [60], and spine degeneration [61], others studies have highlighted the limitations of track-count mapping as a quantitative tool [22, 49, 62–68], including issues related with interpretation of the findings, and variability of the quantitative values.

It could, however, be expected that the use of advanced tracking methods that make the tractogram more quantitative [38–41, 46, 47] might in turn make track-count mapping techniques more suitable for quantitative analysis. In fact, it was recently shown that the spherical-deconvolution informed filtering of tractograms (SIFT) method [39] leads to a more reliable and biological meaningful tractogram [46] and, in turn, making TDI mapping a better quantitative tool, with more interpretable results and lower intra- and

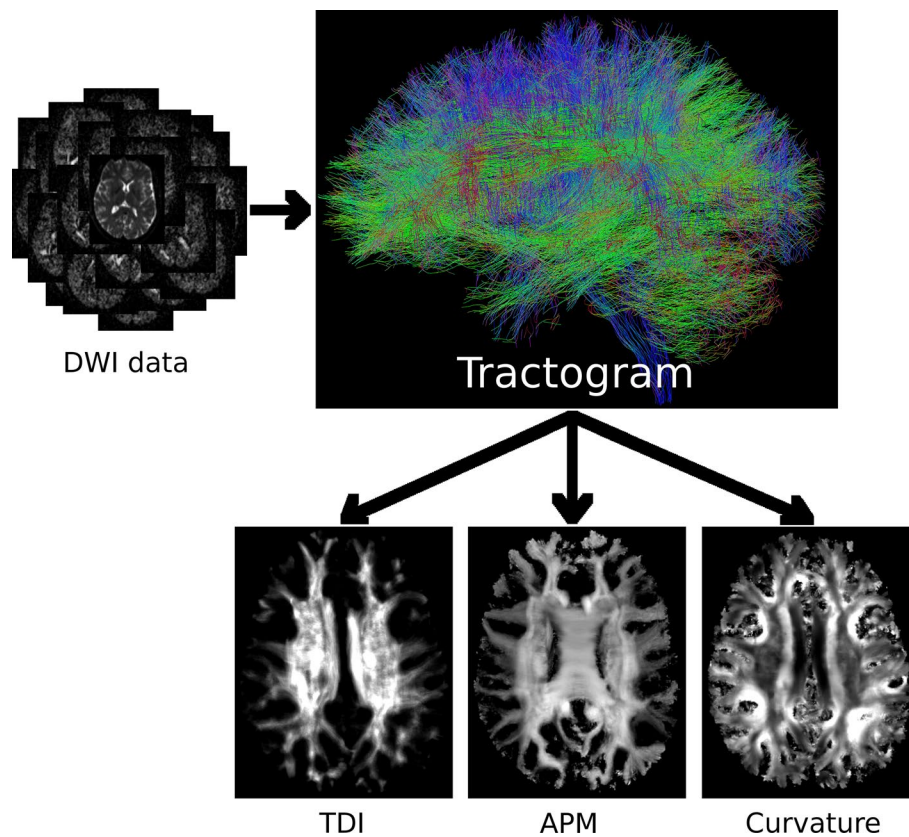


Fig. 9 Example track-weighted imaging (TWI) maps computed solely based on the information contained in the tractogram. The figure summarises the processing pipeline, where diffusion-weighted imaging (DWI) data are used to generate a tractogram, which can then be used to calculate a track-density imaging (TDI) map (*bottom row, left*), an average path-length map (APM) (*bottom row, middle*), or a track-weighted map based on the average local curvature of the streamlines in the voxel (*bottom row, right*). All TWI maps were con-

structed at 0.5 mm isotropic resolution, based on the same diffusion MRI data (acquired at 2.5 mm resolution) and a tractogram of four million streamlines. As appreciated from the figure, each TWI map has unique image contrast and information. For example, the curvature-based TWI map has high intensity in curved bundles (such as sub-cortical U-fibres and the corpus callosum) and low intensity in more straight bundles (such as the portion of the cingulum bundle in that slice)

inter-subject variability [63]. However, that same study [63] also showed that, at native resolution (i.e. without super-resolution), the total apparent fibre density (AFD) [69], corresponding to the orientation average FOD, provides in theory equivalent information to that from a TDI map following SIFT; importantly, since total AFD does not involve a fibre-tracking step, it was shown to have much lower intra- and inter-subject variability than TDI maps calculated either with or without a SIFT step [63]. It was, therefore, concluded that total AFD provides a better option for quantitative analysis of voxel-wise track-count mapping. It should be noted, however, that voxel-wise track-count mapping methods (including total AFD) provide only orientation averaged information and, therefore, discard important information that is retained in other fibre-specific approaches to quantitation [69, 70]. In could, therefore, be argued that fibre-specific approaches are more appropriate for quantifying tract density since they provide increased specificity. Furthermore, recent statistical methods of

connectivity-based enhancement can be used for tract-specific smoothing and enhancement for improved statistical inference [71].

To avoid orientation averaging the TDI information within a voxel, a number of TDI variants have also been proposed, which extend the TWI approach to include both the *spatial* and *angular* domains [39, 72, 73]. They also, therefore, provide fibre-specific information; however, they may still be subject to the length-bias issue if approaches such as SIFT are not used to minimise this effect.

Beyond TDI

Besides mapping the track-count, there are a number of alternative TWI maps that can be generated solely based on properties of the streamlines (see Fig. 9). For example, the technique known as average pathlength mapping (APM) [22] generates a TW image where the intensity at each voxel corresponds to the average length of all the streamlines

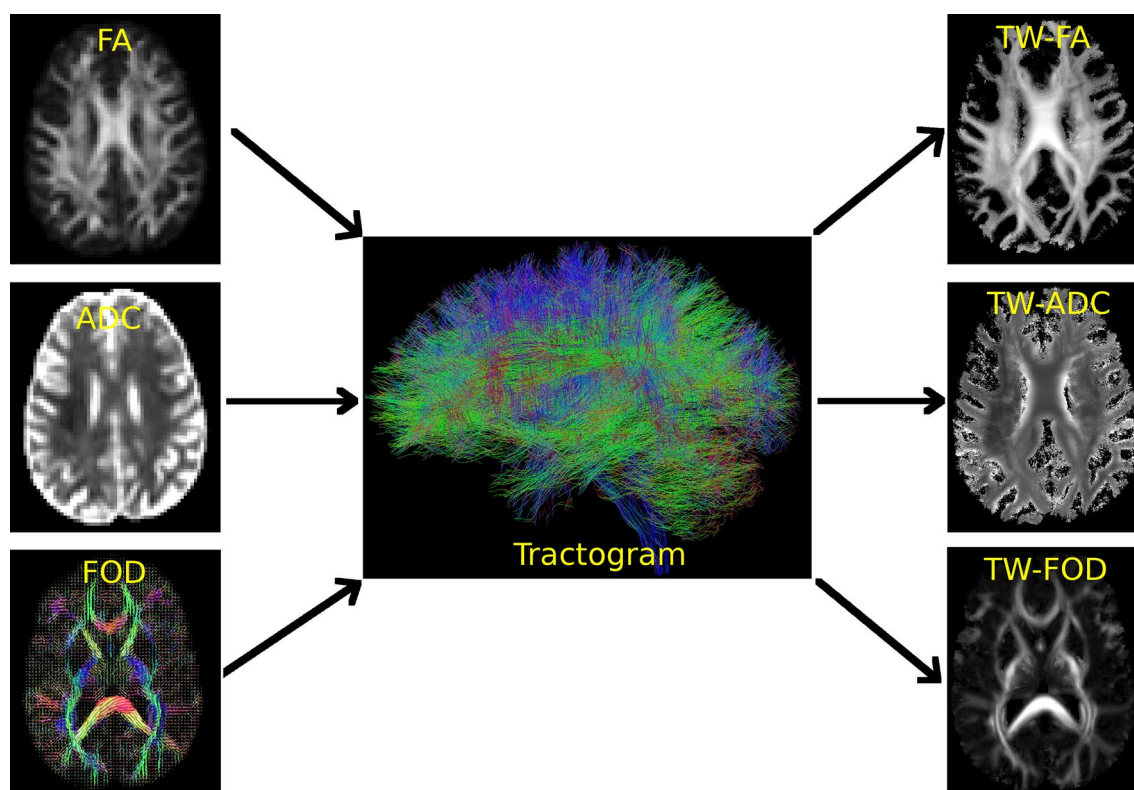


Fig. 10 Example track-weighted imaging (TWI) maps computed by combining the tractogram with other diffusion MRI data. The figure illustrates three cases: in the *top*, a fractional anisotropy (FA) map is combined with the tractogram to compute a TW-FA map; in the *middle*, an apparent diffusion coefficient (ADC) map is combined with the tractogram to compute a TW-ADC map; and in the *bottom*, the fibre orientation distribution (FOD) in each voxel is combined with

the tractogram to compute a TW-FOD map. All TWI maps were constructed at 0.23 mm isotropic resolution, based on the same diffusion MRI data (acquired at 2.3 mm resolution). Each TWI map has unique image contrast and information. Part of this figure is modified from a figure previously published in [17], with permission of Elsevier Inc., 2012)

traversing the voxel. Similarly, other TW maps can be constructed with other properties of the streamlines (e.g. the mean curvature, mean torsion, which can be sensitive to changes in the shape of white matter pathways, regardless of whether there is an associated change in track density or length), or even using other summary statistics (e.g. the length variance of the streamlines instead of their average value). Each of these maps will have very different image contrast, and they all have super-resolution properties (e.g. see Fig. 9).

TWI combining a tractogram with diffusion MRI data

Another approach to generate TW images involves combining the information from the whole-brain tractogram with a map generated from the same diffusion MRI data used to calculate the tractogram. For example, the diffusion MRI data can be used to calculate diffusion tensor based parameters (e.g. average diffusivity, radial and axial diffusivities,

anisotropy measures), and each of these maps can be combined with the tractogram to generate a TW-version of that map (e.g. a tractogram can be combined with a FA map to generate a TW-FA map [17]). In its simplest form, each streamline can be assigned a “weighting” corresponding to the average value measured along the streamline coordinates (e.g. the average FA value along the track), and the final TWI intensity (e.g. the intensity of the TW-FA map) calculated from the mean of these weighting values for all the streamlines traversing a given voxel (see Fig. 10). For this simple implementation, the TWI framework can be considered as a “track-smoothed” version of the corresponding map (in this example, the TW-FA maps is a track-smoothed version of the FA map) [17]. Importantly, this smoothing only occurs along the white matter pathways traversing the voxel (i.e. it can be considered as an “informed” or “smart” smoothing).

The TWI formalism is, however, highly flexible, given that there are many ways in which a tractogram can be combined with another image [17]. For example, the user can determine the extent of the local neighbourhood

that will contribute to calculating the weighting for each streamline (e.g. by selecting the width of a Gaussian weighting function, or selecting a particular maximum track-length when propagating streamlines during the construction of the tractogram, i.e. similar to the case used in *stTDI*). Similarly, the user can choose the track-weighted statistic (e.g. calculating the mean FA value along the track, or the standard deviation of the FA values, or any other metric along the streamline), as well as the *voxel-wise statistic* (e.g. by calculating the mean of the weightings for all the streamlines traversing the voxel, or the variance of the weightings, or their sum), and whether the data are calculated as a scalar value in each voxel or as fibre-specific values [72, 73]. Each of these choices leads to a different image contrast in the resulting TWI maps, which also have super-resolution properties. In the general case (and given the large range of options available when constructing a TWI map), the simple analogy between TWI mapping and a smoothing method is limited, and TWI is better described as “propagating” information (e.g. from the FA map) along the tracks [17].

It should be noted that the tractogram not only can be combined with scalar diffusion MRI maps, but also with other higher-order diffusion MRI data, such as with the fibre orientation distribution (FOD), to generate a TW-FOD map [62] (e.g. see Fig. 10).

One of the advantages of this type of TWI mapping based on combining the tractogram with diffusion MRI data (cf. those described in the sections below) is that the diffusion MRI map used is intrinsically co-registered with the tractogram, and no mis-registration errors are, therefore, present.

All these TWI maps retain the same quantitative characteristics of the diffusion MRI data used to construct them. For example, the TW-ADC map in Fig. 10 has the same units as that of the corresponding ADC map, namely mm^2/s . The TWI maps can therefore be used for the same type of quantitative analysis as that often used for the corresponding diffusion MRI maps (e.g. region-based measurements, tract-of-interest based measurement, histogram analysis, voxel-based analysis).

As an alternative to the local neighbourhood weighting for TWI [17], Bell et al. [74] proposed a TWI variant in which the voxel weight was modulated based on the distance of the voxel from a given anatomical location along the tract (e.g. a segmented region corresponding to a brain abnormality), with a technique they called distance-informed TWI (diTWI).

Several studies have found that many of these TWI maps often have much better reproducibility/variability than that of TDI maps [22, 62, 67] and, therefore, are more suited for quantitation. For example, Willats et al. [62] showed that from all TWI investigated (which included TDI, APM,

TW-ADC, TW-FA, and TW-FOD, with the latter three calculated at three different local neighbourhood extents), TDI had the lowest within-subject quantitative reproducibility and largest between-subject variability. Interestingly, that study also showed that the reproducibility/variability was significantly improved by applying track-weighting (e.g. TW-FA had better reproducibility than FA). They concluded that many of the TWI maps, including APM, TW-ADC, TW-FA, and TW-FOD, have more power to detect group differences for a given effect size, or that they need fewer number of subjects per group to detect a given percentage change [62]. Many of these TWI maps could therefore also play an important role in quantitative analysis.

TWI combining a tractogram with other non-diffusion MRI data

In a similar way to how the tractogram was combined with diffusion MRI data in the previous section, the TWI formalism provides a means to combine the tractogram with other non-diffusion MRI data. For example, the tractogram can be combined with a T_2 map to generate a TW- T_2 map. Similarly, it can be combined with T_1 data, magnetisation transfer data, quantitative susceptibility maps, or any other MRI data, to generate a TW-version of that data/map in each case. Once again, there is flexibility in the choice of local neighbourhood extent, track-weighted statistic, voxel-wise statistic, and the use of a scalar or fibre-specific output. A different image contrast can be achieved in the TW map depending on the particular combination choice for these options. The TWI formalism, therefore, provides a flexible means to combine structural connectivity information (given by the tractogram) with other MRI measurements of tissue properties. Furthermore, as it was the case with TDI, all these TWI variants also have super-resolution properties.

It is important to emphasise, however, that for this type of TWI implementation, co-registration between the diffusion MRI data and the non-diffusion MRI data is essential in order to avoid mis-registration errors; this includes correcting for any image distortions (e.g. eddy currents distortions, and susceptibility-related distortions) or, when this is not possible, at least having matched distortions for both MR imaging modalities; note, however, that, in the latter case, the un-corrected image distortions can introduce significant fibre-tracking errors [75].

TWI combining a tractogram with non-MRI data

A further alternative implementation of TWI involves combining the tractogram with an image generated from data

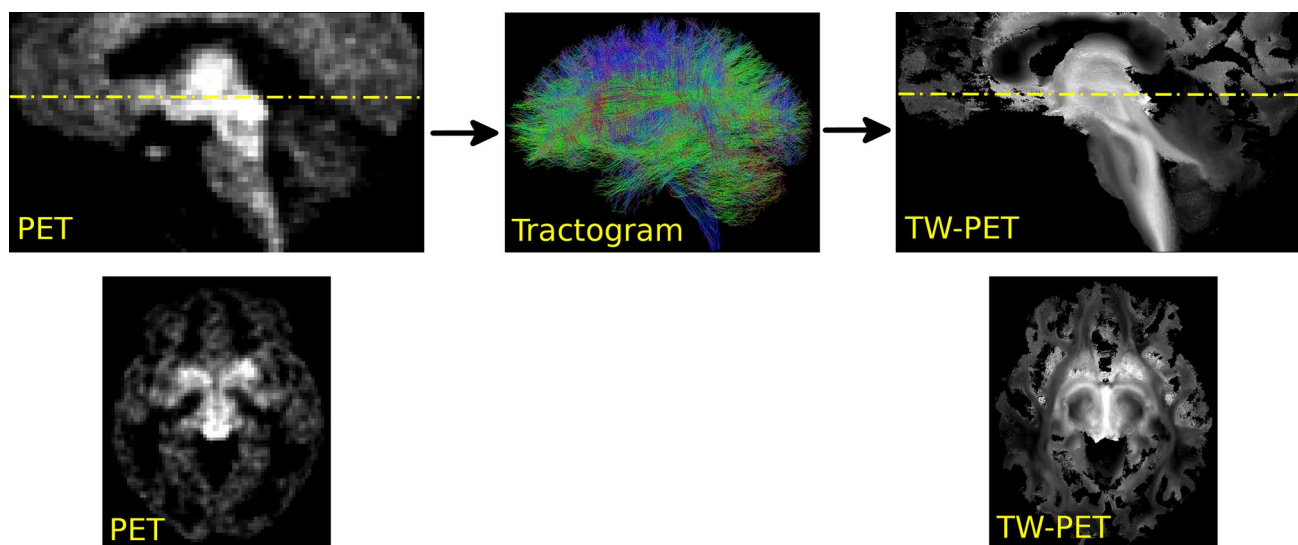


Fig. 11 TWI combining a tractogram and PET data. The *top row* summarises the processing pipeline, where a PET image (in this case, an image based on the ^{11}C -DASB radioligand), is combined with a diffusion MRI tractogram to generate a TW-PET map. In this particular implementation, the TW-PET map can be used to visualise the serotonin pathway, connecting the raphe nuclei (in the brain stem) with the cerebellum, spinal cord and cortical areas. The *bottom row* shows axial slices of the PET and TW-PET data at the level indicated by the *dash-dot line* in the sagittal images in the *top row*. As

other than from MRI (e.g. from PET, SPECT, CT, autoradiography). The TWI framework therefore provides a natural means for fusing multi-modal imaging data. For example, by combining a tractogram with a PET image based on a ^{11}C -DASB radioligand, which has high affinity for serotonin transporters, Calamante et al. [76] generated a TW-PET map that visualised the serotonergic pathway through the raphe nuclei (Fig. 11): by using a very long neighbourhood extent (i.e. the whole length of the streamline), the TW-PET method effectively propagated the PET information along the fibre pathways involved in the ^{11}C -DASB active regions. TW-PET maps, therefore, encode the molecular information from PET and the structural connectivity information from the tractogram, while displaying super-resolution qualities.

As it was the case for the TWI version described in the previous section, this variant of TWI also relies on accurate registration between the various imaging modalities and has the same super-resolution properties.

TWI as a tool to study structural–functional connectivity

A specific TWI case of that described in the section “[TWI combining a tractogram with other non-diffusion MRI data](#)” corresponds to when the non-diffusion MRI data are

can be appreciated in these images, the track-weighted contribution to TW-PET provides high anatomical detail of the network involved in the PET image. TW-PET data were generated at 0.25 mm isotropic resolution, based on 1.8 mm diffusion MRI data acquired at 7 T (see Ref. [76] for further details). Figure constructed from PET and MRI data kindly provided by Prof. Zang-Hee Cho (Neuroscience Research Institute, Gachon University of Medicine and Science, Incheon, Korea)

based on functional MRI. This specific situation can be of great interest because it provides a natural means to combine structural connectivity information (provided by the tractogram) with functional connectivity or functional MRI information (e.g. as provided by BOLD data). In particular, the development of novel methods to investigate brain connectivity and the role they can have to study the interaction between structure and function has received increased interest [77].

By exploiting the TWI formalism, two broad types of TW-functional variants have been proposed. The first variant is based on defining a specific functional network, such as a specific functional connectivity network, the activation network from a block-design fMRI study, or the network generated from an event-related fMRI or EEG-fMRI study. In this variant, the tractogram is then used to compute a track-weighted version of the functional network of interest. For example, in the technique of track-weighted functional connectivity (TW-FC) [78], each streamline in a given voxel was assigned a functional connectivity “weighting” (corresponding to the sum of the functional connectivity values for the chosen network map along the streamline location), and these weightings were then averaged for all the streamlines traversing the voxel. In this way, the functional connectivity information from the network of interest (e.g. the default mode network) is “mapped” to the corresponding white matter pathways and thus TW-FC effectively “propagates” the functional connectivity

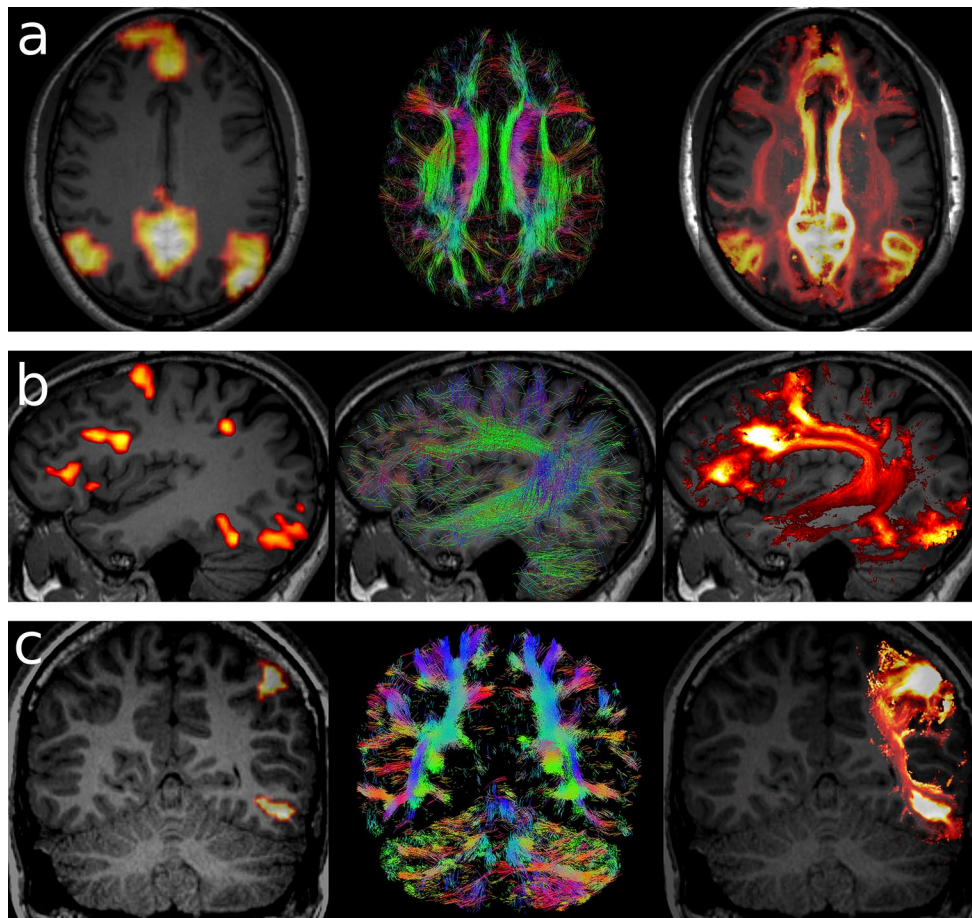


Fig. 12 TWI as a tool to combine structural and functional connectivity information. For each row, the *left* image shows the functional network, the *middle* image the tractogram, and the *right* image the resulting TWI map. **a** Example of the track-weighted functional connectivity (TW-FC) on a healthy subject, generated based on a functional connectivity network (the default mode network in this example). **b** Example of the track-weighted fMRI (TW-fMRI) gen-

erated based on a functional language network (obtained using the orthographic lexical retrieval paradigm in this example). **c** Example of the track-weighted EEG-fMRI (TW-EEGfMRI) on an epilepsy patient with focal cortical dysplasia, generated based on a functional network obtained based on an EEG-fMRI analysis. **b, c** Constructed from images kindly provided by Donna Parker (The Florey Institute of Neuroscience and Mental Health, Melbourne, Australia)

information along the pathways involved in the functional network of interest (Fig. 12a). The TW-FC approach can be directly extended to other functional networks besides functional connectivity, such as in TW-fMRI for networks based on paradigm driven fMRI or TW-EEGfMRI for network based on an EEG-fMRI study; illustrative examples of these two cases are shown in Fig. 12b, c.

The second TW-functional variant does not rely on defining a functional network in advance, but it uses the acquired functional data directly. For example, each streamline in the tractogram can be assigned a functional connectivity “weighting”, which instead of being related to the functional values of a specific network (as it was the case for TW-FC in the first variant), it is based on the Pearson correlation between the BOLD data at the track’s end-points. This approach can be further extended to include dynamic information (by computing the correlation using a sliding

window approach [79]), in a technique referred to as track-weighted dynamic functional connectivity (TW-dFC) [80]. In this way, the TWI formalism can be used to combine structural and functional information into a four dimensional dataset, which can be used to study dynamic functional connectivity based on the combined structural/functional information. In particular, these TW-dFC data were shown to provide a powerful means to achieve tissue parcellation in a data-driven way, by exploiting the combined information of structural, functional and dynamic connectivity [80].

As mentioned for many of the other TWI variants, the TWI output does not have to be necessarily a scalar map (i.e. by orientation averaging the information from all the fibres in the voxel), but it can also be stored as a fibre-specific TW data. As illustration, Fig. 13 shows the fibre-specific output for the case of TW-fMRI based on an fMRI language paradigm (same subject as that shown for the scalar TWI output in Fig. 12b).

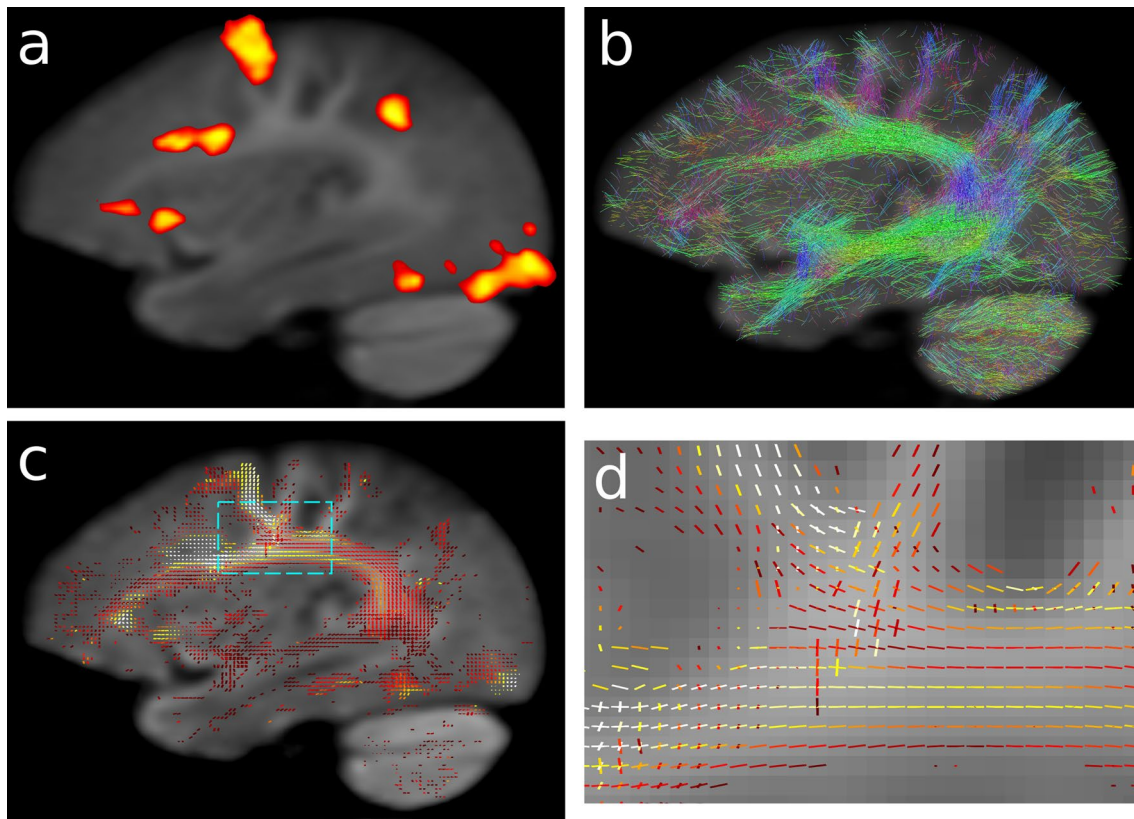


Fig. 13 Example of fibre-specific version of the TWI output. The example corresponds to the TW-fMRI map generated by combining an fMRI language network (a) with a tractogram (b). c Fibre-specific TW-fMRI map, with the *dashed rectangle* indicating the zoomed region showed in d. The data are for the same subject as that shown in the scalar TWI output in Fig. 12b. As can be appreciated, each

voxel has a specific TW-fMRI value assigned to each fibre population (represented by the *lines* in each voxel), and no orientation averaging has been performed (cf. TW-fMRI map in Fig. 12b). Figure constructed from images kindly provided by Donna Parker (The Florey Institute of Neuroscience and Mental Health, Melbourne, Australia)

Practical issues

Tractography choices

Since TWI maps are images of the tractogram (or weighted-images of the tractogram), there are a number of factors affecting the tractogram that will, therefore, have a corresponding effect on the TWI maps. For example, Fig. 7 illustrated a possible effect of the choice of tractography algorithm on the resulting TDI map. Similarly, other fibre-tracking algorithm-specific choices, known to influence the resulting tractogram (such as the step-size, curvature constraints, seeding mask, termination criteria, use of interpolation, etc.) [1, 4, 38, 49, 68, 81–83], will also lead to corresponding effects on TWI maps. The reader is referred to these studies for more details regarding the various factors that can affect the tractogram, their consequences, and how they can be reduced.

A related issue to consider is the relationship between the step-size and the chosen super-resolution for the TWI

map. While at first sight it would appear that the step-size of the tractography algorithm should be smaller than the TWI voxel size, this is not necessarily the case in practice. It is important to select the step-size small enough to minimise the bias (i.e. overshoot) when tracking curved structures [82–84]. However, the step-size can be larger than the TWI resolution. For example, the MRtrix (<http://www.mrtrix.org>) implementation of TWI mapping upsamples streamlines by local interpolation, to ensure that sufficient sampling points are included within each super-resolution voxel (e.g. the maximum inter-point distance set to a fraction of the super-resolution voxel size).

Number of tracks vs. super-resolution voxel size

Similarly to the relationship between the number of samples and the bin size in the case of a histogram plot (i.e. the smaller the bin size, the larger the number of samples required in order to properly characterise the histogram distribution), TWI requires a larger number of streamlines

in the tractogram when using a smaller super-resolution voxel size. In other words, the smaller the voxel size, the denser the tractogram must be in order to have a sufficient large number of streamlines in each voxel to calculate a meaningful track-weighted metric (e.g. the mean values of the streamlines' weightings in the voxel). In the author's experience, a tractogram of ~5 to 10 million probabilistic streamlines provides high-quality TWI maps at super-resolution voxels of ~0.2 to 0.5 mm isotropic for typical human brain diffusion MRI data.

For the specific case of using the short-tracks version, e.g. *stTDI* [24], the total number of streamlines in the tractogram must be greatly increased (e.g. by an order of magnitude), given that each streamline has now been stopped after a short propagation length (e.g. 10 times the acquired voxel size), and therefore, it will only contribute track-weighting information to fewer super-resolution voxels. It should be noted, however, that neither the computation time to generate the tractogram nor the file size will necessarily be very different: each short streamline is computed much quicker and occupies less space in storage.

Interpretation: local vs. distant effect

As emphasised in the original TDI publication [19], it is important to emphasise that a change observed in a given location in the TWI map may be due to a local effect (e.g. a lesion in that location) or to a distant effect (e.g. a change affecting the tracks connecting to that location, such as a distant abnormality that disrupted that connection, or the presence of extra tracks to the location of interest [63]). As a possible way to investigate these two scenarios, it is for example recommended to use the detected area of TWI change as a seed region for targeted tracking (or, alternatively, to track-edit the tractogram using the abnormal TWI region to isolate the streamlines of interest); in this way, the brain areas that have contributed to the detected TWI change can be identified.

Focal vs. extended abnormalities

As discussed above (see “[TWI combining a tractogram with diffusion MRI data](#)” section), there are a number of ways to control the spatial extent (along the streamline) that will contribute to the weighting assigned to each streamline (i.e. the size of the local neighbourhood), including using a Gaussian weighting function along the streamline, or selecting a specific maximum track-length when constructing the tractogram). The particular choice for a given study will depend on the expected abnormality. For example, if a disease is expected to affect a large extent of a white matter pathway, then the use of large local neighbourhood is

likely to be beneficial. In contrast, for cases where only focal abnormalities in white matter are expected, then a small local neighbourhood (e.g. a narrow Gaussian weighting function or the use of a short-track tractogram) should be favourable [17].

Choice of resolution

An issue of interest is the level of super-resolution that can be achieved in practice using TWI. It should be noted that TWI creates a map of the tractogram (e.g. a histogram of streamlines count for TDI, or a map of the average streamlines length for APM, or a TW version of a given parameter for many other TWI maps). Therefore, while any super-resolution voxel-size can, in principle, be used, in practice only features that are present in the tractogram will be able to be resolved. For example, if the diffusion MRI data quality is not sufficient to reconstruct the streamlines from a small white matter pathway, then that white matter structure will not be able to be resolved regardless of the choice of super-resolution voxel-size. On the other hand, if a white matter pathway is represented as a separate structure in the tractogram, TWI will also be able to resolve it at high resolution.

Another interesting scenario is that of a very small white matter abnormality, smaller than the acquired diffusion MRI voxel size. This small focal abnormality is likely to be invisible to TWI regardless of the super-resolution size chosen: as explained in the Section “[TW images based solely on properties of the tractogram](#)”, the super-resolution property relies on the continuity of the streamlines bringing information from outside the voxel, in order to resolve intra-voxel information; for the case of a focal sub-voxel lesion, no extra-voxel information is available.

Voxel-based analysis: statistical methods

It should be noted that the signal intensity of TWI maps at different locations are not necessarily independent, i.e. the track-weighting propagates the information along the pathways and, therefore, the values in regions that have common white matter pathways cannot be considered independent. Standard parametric methods for voxel-based comparisons, such as those commonly used in SPM [85], are, therefore, not likely to be appropriate, and permutation-based testing strategies [86, 87] are more applicable. Importantly, given that by the track-weighting process, information is propagated along white matter pathways in TWI, statistical significance should be considered using cluster-based inference. In particular, a method recently developed for fibre-specific voxel-based analysis of FOD-based measures, which boosts the statistical inference based on connectivity-based enhancement, a technique

referred to as connectivity-based fixel enhancement [71],⁵ should provide a powerful statistical approach for voxel-wise comparison of (orientation averaged and fibre-specific) TWI measures.

TWI warping: warp tracks vs. warp TWI maps

When TWI maps need to be warped to template space (e.g. for group analysis), there are in principle two possible approaches: warp the tractogram and then calculate the TWI map in template space, or calculate the TWI map in subject space and then warp the resulting map to a template. It should be noted that for some TWI maps, such as TDI-based maps, these two approaches are not equivalent [78]. The normalisation step to a TDI map can lead to compression or expansion of white matter structures, which in turn can lead to changes in streamlines density; this unfortunately cannot be compensated by using the Jacobian of the transformation, given that the change in streamline density depends on the orientation of the white matter pathway relative to direction of compression/expansion [22, 78]. It is therefore important that TDI-based maps are not directly normalised, but rather that the normalisation is applied to the tractogram. For the case of TWI maps that are not based on streamline density measures (e.g. TW-FA, TW-PET, TW-FC, among many others non-TDI maps), either approach (i.e. normalising the tractogram or normalising the TWI maps) should be equivalent.

Power calculations

As discussed by Willats et al. [62], power calculations based on TWI are not straightforward, given that TWI maps are spatially correlated (e.g. due to the track-weighted process and the use of neighbourhood information), which limits the number of independent tests. Furthermore, power calculations within a permutation-based cluster analysis framework are non-trivial because the choice of sample size modifies the form of the distribution. Simpler power calculations based on the Bonferroni correction have been used, but this only provides very conservative sample and effect size estimates, since they assume that all tests are independent [62].

Conclusion

Track-weighted imaging provides a very flexible framework, where one tractogram can be used to generate many different possible images, each of them with very different image

contrast, all with super-resolution properties. TWI can be constructed based solely on properties of the tractogram, or by combining the tractogram with other diffusion MRI map, with a non-diffusion MRI data, or even with a non-MRI data set. At the centre of all these TW images is the tractogram and, therefore, the better the quality of the tractogram, the better the quality of the resulting TW images. The particular choice of TWI variant and implementation will depend on the application of interest. For example, for high resolution and high-anatomical detail, super-resolution TDI might be the TWI of choice, while for molecular imaging the combination of structural information and the specificity provided by radiolabelled molecules in TW-PET should be of great interest. All the TWI results presented in this review article were generated using the freeware MRtrix (<http://www.mrtrix.org>).

Acknowledgements We are grateful to the many colleagues and collaborators involved in the track-weighted imaging work, and in particular to Alan Connelly, Jacques-Donald Tournier, and Robert E. Smith for their extensive contribution to developing these methods. We are also grateful to Chun-Hung Yeh and Donna Parker for help in producing figures for this work. We thank the National Health and Medical Research Council (NHMRC) of Australia, the Australian Research Council (ARC), and the Victorian Government's Operational Infrastructure Support Grant for their support.

Compliance with ethical standards

Conflict of interest FC is co-inventor in a patent application on the TDI method.

Funding This study was funded by the National Health and Medical Research Council (NHMRC) of Australia, the Australian Research Council (ARC), and the Victorian Government's Operational Infrastructure Support Grant.

References

1. Tournier J-D, Mori S, Leemans A (2011) Diffusion tensor imaging and beyond. *Magn Reson Med* 65:1532–1556
2. Mori S, Crain BJ, Chacko VP, van Zijl PC (1999) Three-dimensional tracking of axonal projections in the brain by magnetic resonance imaging. *Ann Neurol* 45:265–269
3. Conturo TE, Lori NF, Cull TS, Akbudak E, Snyder AZ, Shimony JS, McKinstry RC, Burton H, Raichle ME (1999) Tracking neuronal fiber pathways in the living human brain. *Proc Natl Acad Sci USA* 96:10422–10427
4. Tournier J-D, Calamante F, Connelly A (2012) MRtrix: diffusion tractography in crossing fiber regions. *Int J Imaging Syst Technol* 22:53–66
5. Behrens TEJ, Johansen-Berg H, Woolrich MW, Smith SM, Wheeler-Kingshott CAM, Boulby PA, Barker GJ, Sillery EL, Sheehan K, Ciccarelli O, Thompson AJ, Brady JM, Matthews PM (2003) Non-invasive mapping of connections between human thalamus and cortex using diffusion imaging. *Nat Neurosci* 6:750–757
6. Hagmann P, Kurant M, Gigandet X, Thiran P, Wedeen VJ, Meuli R, Thiran J-P (2007) Mapping human whole-brain structural networks with diffusion MRI. *PLoS One* 2:e597

⁵ The term “fixel” was introduced in that paper to refer to a specific fibre population within a single voxel.

7. Fornito A, Zalesky A, Breakspear M (2013) Graph analysis of the human connectome: promise, progress, and pitfalls. *Neuroimage* 80:426–444
8. Fornito A, Zalesky A, Breakspear M (2015) The connectomics of brain disorders. *Nat Rev Neurosci* 16:159–172
9. Correia S, Lee SY, Voorn T, Tate DF, Paul RH, Zhang S, Salloy SP, Malloy PF, Laidlaw DH (2008) Quantitative tractography metrics of white matter integrity in diffusion-tensor MRI. *Neuroimage* 42:568–581
10. Berman JI, Mukherjee P, Partridge SC, Miller SP, Ferriero DM, Barkovich AJ, Vigneron DB, Henry RG (2005) Quantitative diffusion tensor MRI fiber tractography of sensorimotor white matter development in premature infants. *Neuroimage* 27:862–871
11. Jones DK, Travis AR, Eden G, Pierpaoli C, Basser PJ (2005) PASTA: pointwise assessment of streamline tractography attributes. *Magn Reson Med* 53:1462–1467
12. Yeatman JD, Dougherty RF, Myall NJ, Wandell BA, Feldman HM (2012) Tract profiles of white matter properties: automating fiber-tract quantification. *PLoS One* 7:e49790
13. Colby JB, Soderberg L, Lebel C, Dinov ID, Thompson PM, Sowell ER (2012) Along-tract statistics allow for enhanced tractography analysis. *Neuroimage* 59:3227–3242
14. Mezer A, Yeatman JD, Stikov N, Kay KN, Cho N-J, Dougherty RF, Perry ML, Parvizi J, Hua LH, Butts-Paully K, Wandell BA (2013) Quantifying the local tissue volume and composition in individual brains with magnetic resonance imaging. *Nat Med* 19:1667–1672
15. Travis KE, Golden NH, Feldman HM, Solomon M, Nguyen J, Mezer A, Yeatman JD, Dougherty RF (2015) Abnormal white matter properties in adolescent girls with anorexia nervosa. *Neuroimage Clin* 9:648–659
16. Batchelor PG, Calamante F, Tournier J-D, Atkinson D, Hill DLG, Connelly A (2006) Quantification of the shape of fiber tracts. *Magn Reson Med* 55:894–903
17. Calamante F, Tournier J-D, Smith RE, Connelly A (2012) A generalised framework for super-resolution track-weighted imaging. *Neuroimage* 59:2494–2503
18. Embleton K, Morris D, Haroon H, Lambon Ralph M (2007) Anatomical Connectivity Mapping. Proceedings of the International Society for Magnetic Resonance in Medicine (ISMRM), 15th Annual Meeting, Berlin, Germany, (pp 19–25 May 1548)
19. Calamante F, Tournier J-D, Jackson GD, Connelly A (2010) Track-density imaging (TDI): super-resolution white matter imaging using whole-brain track-density mapping. *Neuroimage* 53:1233–1243
20. Bozzali M, Parker GJM, Serra L, Embleton K, Gili T, Perri R, Caltagirone C, Cercignani M (2011) Anatomical connectivity mapping: a new tool to assess brain disconnection in Alzheimer's disease. *Neuroimage* 54:2045–2051
21. Stadlbauer A, Buchfelder M, Salomonowitz E, Ganslandt O (2010) Fiber density mapping of gliomas: histopathologic evaluation of a diffusion-tensor imaging data processing method. *Radiology* 257:846–853
22. Pannek K, Mathias JL, Bigler ED, Brown G, Taylor JD, Rose SE (2011) The average pathlength map: a diffusion MRI tractography-derived index for studying brain pathology. *Neuroimage* 55:133–141
23. Calamante F, Tournier J-D, Heidemann RM, Anwender A, Jackson GD, Connelly A (2011) Track density imaging (TDI): validation of super resolution property. *Neuroimage* 56:1259–1266
24. Calamante F, Tournier J-D, Kurniawan ND, Yang Z, Gyengesi E, Galloway GJ, Reutens DC, Connelly A (2012) Super-resolution track-density imaging studies of mouse brain: comparison to histology. *Neuroimage* 59:286–296
25. Pajevic S, Pierpaoli C (2000) Color schemes to represent the orientation of anisotropic tissues from diffusion tensor data: application to white matter fiber tract mapping in the human brain. *Magn Reson Med* 43:921
26. Dhollander T, Smith R, Tournier J-D, Jeurissen B, Connelly A (2015) Time to move on: an FOD-based DEC map to replace DTI's trademark DEC FA. Proceedings of International Society for Magnetic Resonance in Medicine (ISMRM), 23rd Annual Meeting, Toronto, Canada 1027
27. Calamante F, Oh S-H, Tournier J-D, Park S-Y, Son Y-D, Chung J-Y, Chi J-G, Jackson GD, Park C-W, Kim Y-B, Connelly A, Cho Z-H (2013) Super-resolution track-density imaging of thalamic substructures: comparison with high-resolution anatomical magnetic resonance imaging at 7.0T. *Hum Brain Mapp* 34:2538–2548
28. Cho ZH, Calamante F, Chi JG (2015) 7.0 Tesla MRI brain white matter atlas, 2nd edn. Springer, New York
29. Hoch MJ, Chung S, Ben-Eliezer N, Bruno MT, Fatterpekar GM, Shepherd TM (2016) New clinically feasible 3T MRI protocol to discriminate internal brain stem anatomy. *Am J Neuroradiol* 37:1058–1065
30. Wenz H, Al-Zghloul M, Hart E, Kurth S, Groden C, Förster A (2016) Track-density imaging of the human brainstem for anatomic localization of fiber tracts and nerve nuclei in Vivo: initial experience with 3-T magnetic resonance imaging. *World Neurosurg* 93:286–292
31. Palesi F, Tournier J-D, Calamante F, Muhlert N, Castellazzi G, Chard D, D'Angelo E, Wheeler-Kingshott CAM (2015) Contralateral cerebello-thalamo-cortical pathways with prominent involvement of associative areas in humans in vivo. *Brain Struct Funct* 220:3369–3384
32. Kurniawan ND, Richards KL, Yang Z, She D, Ullmann JFP, Moldrich RX, Liu S, Yaksic JU, Leanage G, Kharatishvili I, Wimmer V, Calamante F, Galloway GJ, Petrou S, Reutens DC (2014) Visualization of mouse barrel cortex using ex vivo track density imaging. *Neuroimage* 87:465–475
33. Richards K, Calamante F, Tournier J-D, Kurniawan ND, Sadeghian F, Retchford AR, Jones GD, Reid CA, Reutens DC, Ordidge R, Connelly A, Petrou S (2014) Mapping somatosensory connectivity in adult mice using diffusion MRI tractography and super-resolution track density imaging. *Neuroimage* 102(Pt 2):381–392
34. Ullmann JFP, Calamante F, Collin SP, Reutens DC, Kurniawan ND (2015) Enhanced characterization of the zebrafish brain as revealed by super-resolution track-density imaging. *Brain Struct Funct* 220:457–468
35. Hamaide J, De Groof G, Van Steenkiste G, Jeurissen B, Van Audekerke J, Naeyaert M, Van Ruijssevelt L, Cornil C, Sijbers J, Verhoye M, Van der Linden A (2016) Exploring sex differences in the adult zebra finch brain: in vivo diffusion tensor imaging and ex vivo super-resolution track density imaging. *Neuroimage*. doi:10.1016/j.neuroimage.2016.09.067
36. Tournier J-D, Calamante F, Connelly A (2007) Robust determination of the fibre orientation distribution in diffusion MRI: non-negativity constrained super-resolved spherical deconvolution. *Neuroimage* 35:1459–1472
37. Farquharson S, Tournier J-D, Calamante F, Fabinyi G, Schneider-Kolsky M, Jackson GD, Connelly A (2013) White matter fiber tractography: why we need to move beyond DTI. *J Neurosurg* 118:1367–1377
38. Smith RE, Tournier J-D, Calamante F, Connelly A (2012) Anatomically-constrained tractography: improved diffusion MRI streamlines tractography through effective use of anatomical information. *Neuroimage* 62:1924–1938
39. Smith RE, Tournier J-D, Calamante F, Connelly A (2013) SIFT: spherical-deconvolution informed filtering of tractograms. *Neuroimage* 67:298–312

40. Reisert M, Mader I, Anastasopoulos C, Weigel M, Schnell S, Kiselev V (2011) Global fiber reconstruction becomes practical. *Neuroimage* 54:955–962
41. Daducci A, Dal Palù A, Descoteaux M, Thiran J-P (2016) Microstructure Informed Tractography: pitfalls and open challenges. *Front Neurosci* 10:247
42. Sotiropoulos SN, Jbabdi S, Xu J, Andersson JL, Moeller S, Auerbach EJ, Glasser MF, Hernandez M, Sapiro G, Jenkinson M, Feinberg DA, Yacoub E, Lenglet C, Van Essen DC, Ugurbil K, Behrens TEJ, WU-Minn HCP Consortium (2013) Advances in diffusion MRI acquisition and processing in the human connectome project. *Neuroimage* 80:125–143
43. McNab JA, Edlow BL, Witzel T, Huang SY, Bhat H, Heberlein K, Feiweier T, Liu K, Keil B, Cohen-Adad J, Tisdall MD, Folkner RD, Kinney HC, Wald LL (2013) The Human Connectome Project and beyond: initial applications of 300 mT/m gradients. *Neuroimage* 80:234–245
44. Jeurissen B, Tournier J-D, Dhollander T, Connelly A, Sijbers J (2014) Multi-tissue constrained spherical deconvolution for improved analysis of multi-shell diffusion MRI data. *Neuroimage* 103:411–426
45. Smith RE, Tournier J-D, Calamante F, Connelly A (2015) SIFT2: enabling dense quantitative assessment of brain white matter connectivity using streamlines tractography. *Neuroimage* 119:338–351
46. Smith RE, Tournier J-D, Calamante F, Connelly A (2015) The effects of SIFT on the reproducibility and biological accuracy of the structural connectome. *Neuroimage* 104:253–265
47. Daducci A, Dal Palù A, Lemkaddem A, Thiran J-P (2015) COMMIT: convex optimization modeling for microstructure informed tractography. *IEEE Trans Med Imaging* 34:246–257
48. Girard G, Whittingstall K, Deriche R, Descoteaux M (2014) Towards quantitative connectivity analysis: reducing tractography biases. *Neuroimage* 98:266–278
49. Jones DK (2010) Challenges and limitations of quantifying brain connectivity in vivo with diffusion MRI. *Imaging Med* 2:341–355
50. Li L, Rilling JK, Preuss TM, Glasser MF, Hu X (2012) The effects of connection reconstruction method on the interregional connectivity of brain networks via diffusion tractography. *Hum Brain Mapp* 33:1894–1913
51. Barajas RF, Hess CP, Phillips JJ, Von Morze CJ, Yu JP, Chang SM, Nelson SJ, McDermott MW, Berger MS, Cha S (2013) Super-resolution track density imaging of glioblastoma: histopathologic correlation. *Am J Neuroradiol* 34:1319–1325
52. Stadlbauer A, Hammen T, Grummich P, Buchfelder M, Kuwert T, Dörfler A, Nimsky C, Ganslandt O (2011) Classification of peritumoral fiber tract alterations in gliomas using metabolic and structural neuroimaging. *J Nucl Med* 52:1227–1234
53. Ziegler E, Rouillard M, André E, Coolen T, Stender J, Balteau E, Phillips C, Garraux G (2014) Mapping track density changes in nigrostriatal and extranigral pathways in Parkinson's disease. *Neuroimage* 99:498–508
54. Bozzali M, Parker GJM, Spanò B, Serra L, Giulietti G, Perri R, Magnani G, Marra C, Vita GM, Caltagirone C, Cercignani M (2013) Brain tissue modifications induced by cholinergic therapy in Alzheimer's disease. *Hum Brain Mapp* 34:3158–3167
55. Bozzali M, Spanò B, Parker GJM, Giulietti G, Castelli M, Basile B, Rossi S, Serra L, Magnani G, Nocentini U, Caltagirone C, Centonze D, Cercignani M (2013) Anatomical brain connectivity can assess cognitive dysfunction in multiple sclerosis. *Mult Scler* 19:1161–1168
56. Lyksborg M, Siebner HR, Sørensen PS, Blinkenberg M, Parker GJM, Dagonowski A-M, Garde E, Larsen R, Dyrby TB (2014) Secondary progressive and relapsing remitting multiple sclerosis leads to motor-related decreased anatomical connectivity. *PLoS One* 9:e95540
57. Tan XL, Wright DK, Liu S, Hovens C, O'Brien TJ, Shultz SR (2016) Sodium selenate, a protein phosphatase 2A activator, mitigates hyperphosphorylated tau and improves repeated mild traumatic brain injury outcomes. *Neuropharmacology* 108:382–393
58. Vaessen MJ, Saj A, Lovblad K-O, Gschwind M, Vuilleumier P (2016) Structural white-matter connections mediating distinct behavioral components of spatial neglect in right brain-damaged patients. *Cortex* 77:54–68
59. Stadlbauer A, Ganslandt O, Salomonowitz E, Buchfelder M, Hammen T, Bachmair J, Eberhardt K (2012) Magnetic resonance fiber density mapping of age-related white matter changes. *Eur J Radiol* 81:4005–4012
60. Woodworth D, Mayer E, Leu K, Ashe-McNalley C, Naliboff BD, Labus JS, Tillisch K, Kutch JJ, Farmer MA, Apkarian AV, Johnson KA, Mackey SC, Ness TJ, Landis JR, Deutsch G, Harris RE, Clauw DJ, Mullins C, Ellingson BM, MAPP Research Network (2015) Unique Mmicrostructural changes in the brain associated with urological chronic pelvic pain syndrome (UCPPS) revealed by diffusion tensor MRI, super-resolution track density imaging, and statistical parameter mapping: a MAPP network neuroimaging study. *PLoS One* 10:e0140250
61. Ellingson BM, Salamon N, Woodworth DC, Holly LT (2015) Correlation between degree of subvoxel spinal cord compression measured with super-resolution tract density imaging and neurological impairment in cervical spondylotic myelopathy. *J Neurosurg Spine* 22:631–638
62. Willats L, Raffelt D, Smith RE, Tournier J-D, Connelly A, Calamante F (2013) Quantification of track-weighted imaging (TWI): characterisation of within-subject reproducibility and between-subject variability. *Neuroimage* 87:18–31
63. Calamante F, Smith RE, Tournier J-D, Raffelt D, Connelly A (2015) Quantification of voxel-wise total fibre density: investigating the problems associated with track-count mapping. *Neuroimage* 117:284–293
64. Calamante F (2016) Super-resolution track density imaging: anatomic detail versus quantification. *Am J Neuroradiol* 37:1066–1067
65. Besseling RMH, Jansen JFA, Overvliet GM, Vaessen MJ, Braakman HMH, Hofman PAM, Aldenkamp AP, Backes WH (2012) Tract specific reproducibility of tractography based morphology and diffusion metrics. *PLoS One* 7:e34125
66. Bloy L, Ingalhalikar M, Batmanghelich NK, Schultz RT, Roberts TPL, Verma R (2012) An integrated framework for high angular resolution diffusion imaging-based investigation of structural connectivity. *Brain Connect* 2:69–79
67. Pannek K, Mathias JL, Rose SE (2011) MRI diffusion indices sampled along streamline trajectories: quantitative tractography mapping. *Brain Connect* 1:331–338
68. Jones DK, Knösche TR, Turner R (2013) White matter integrity, fiber count, and other fallacies: the do's and don'ts of diffusion MRI. *Neuroimage* 73:239–254
69. Raffelt D, Tournier J-D, Rose S, Ridgway GR, Henderson R, Crozier S, Salvado O, Connelly A (2012) Apparent Fibre Density: a novel measure for the analysis of diffusion-weighted magnetic resonance images. *Neuroimage* 59:3976–3994
70. Dell'Acqua F, Simmons A, Williams SCR, Catani M (2013) Can spherical deconvolution provide more information than fiber orientations? Hindrance modulated orientational anisotropy, a true-tract specific index to characterize white matter diffusion. *Hum Brain Mapp* 34:2464–2483
71. Raffelt DA, Smith RE, Ridgway GR, Tournier J-D, Vaughan DN, Rose S, Henderson R, Connelly A (2015) Connectivity-based fixel enhancement: whole-brain statistical analysis of diffusion MRI measures in the presence of crossing fibres. *Neuroimage* 117:40–55

72. Pannek K, Raffelt D, Salvado O, Rose S (2012) Incorporating directional information in diffusion tractography derived maps: angular track imaging (ATI). Proceedings of the International Society for Magnetic Resonance in Medicine (ISMRM), 20th Annual Meeting, Toronto, Canada, vol 1912, pp 5–11
73. Dhollander T, Emsell L, Van Hecke W, Maes F, Suetens S, Suetens P (2014) Track orientation density imaging (TODI) and track orientation distribution (TOD) based tractography. *Neuroimage* 94:312–336
74. Bell C, Pannek K, Fay M, Thomas P, Bourgeat P, Salvado O, Gal Y, Coulthard A, Crozier S, Rose S (2014) Distance informed track-weighted imaging (diTWI): a framework for sensitising streamline information to neuropathology. *Neuroimage* 86:60–66
75. Irfanoglu MO, Walker L, Sarlls J, Marengo S, Pierpaoli C (2012) Effects of image distortions originating from susceptibility variations and concomitant fields on diffusion MRI tractography results. *Neuroimage* 61:275–288
76. Calamante F, Son Y-D, Tournier J-D, Ryu T-H, Oh S-H, Connelly A, Cho Z-H (2012) Fusing PET and MRI Data Using super-resolution track-weighted imaging. Proceedings of the International Society for Magnetic Resonance in Medicine (ISMRM), 20th Annual Meeting, Toronto, Canada, vol 1919, pp 5–11
77. Smith S (2013) Introduction to the NeuroImage special issue “Mapping the Connectome”. *Neuroimage* 80:1
78. Calamante F, Masterton RAJ, Tournier J-D, Smith RE, Willats L, Raffelt D, Connelly A (2013) Track-weighted functional connectivity (TW-FC): a tool for characterizing the structural–functional connections in the brain. *Neuroimage* 70:199–210
79. Hutchison RM, Womelsdorf T, Allen EA, Bandettini PA, Calhoun VD, Corbetta M, Della Penna S, Duyn JH, Glover GH, Gonzalez-Castillo J, Handwerker DA, Keilholz S, Kiviniemi V, Leopold DA, de Pasquale F, Sporns O, Walter M, Chang C (2013) Dynamic functional connectivity: promise, issues, and interpretations. *Neuroimage* 80:360–378
80. Calamante F, Smith RE, Liang X, Zalesky A, Connelly A (2016) Track-weighted dynamic functional connectivity (TW-dFC): a new method to study dynamic connectivity. In: Proceedings of the international society for magnetic resonance in medicine (ISMRM), 24th Annual Meeting, Singapore, vol 308, pp 7–13
81. Mori S, van Zijl PCM (2002) Fiber tracking: principles and strategies—a technical review. *NMR Biomed* 15:468–480
82. Lazar M, Alexander AL (2003) An error analysis of white matter tractography methods: synthetic diffusion tensor field simulations. *Neuroimage* 20:1140–1153
83. Tournier J-D, Calamante F, King MD, Gadian DG, Connelly A (2002) Limitations and requirements of diffusion tensor fiber tracking: an assessment using simulations. *Magn Reson Med* 47:701–708
84. Basser PJ, Pajevic S, Pierpaoli C, Duda J, Aldroubi A (2000) In vivo fiber tractography using DT-MRI data. *Magn Reson Med* 44:625–632
85. Ashburner J, Friston KJ (2000) Voxel-based morphometry—the methods. *Neuroimage* 11:805–821
86. Nichols TE, Holmes AP (2002) Nonparametric permutation tests for functional neuroimaging: a primer with examples. *Hum Brain Mapp* 15:1–25
87. Hayasaka S, Nichols TE (2004) Combining voxel intensity and cluster extent with permutation test framework. *Neuroimage* 23:54–63